

Softmax-free Linear Transformers

Jiachen Lu¹, · Junge Zhang¹, · Xiatian Zhu², · Jiafeng Feng¹, · Tao Xiang², · Li Zhang¹✉

Abstract Vision transformers (ViTs) have pushed the state-of-the-art for visual perception tasks. The self-attention mechanism underpinning the strength of ViTs has a quadratic complexity in both computation and memory usage. This motivates the development of approximating the self-attention at linear complexity. However, an in-depth analysis in this work reveals that existing methods are either theoretically flawed or empirically ineffective for visual recognition. We identify that their limitations are rooted in the inheritance of *softmax* based self-attention during approximations, that is, normalizing the scaled dot-product between token feature vectors using the softmax function. As preserving the softmax operation challenges any subsequent linearization efforts. By this insight, a family of *SOFTmax-Free Transformers* (**SOFT**) are proposed. Specifically, a Gaussian kernel function is adopted to replace the dot-product similarity, enabling a full self-attention matrix to be approximated under low-rank matrix decomposition. For computational robustness, we estimate the Moore-Penrose inverse using an iterative Newton-Raphson method in the forward process only, while calculating its theoretical gradients only once in the backward process. To further expand applicability (*e.g.*, dense prediction tasks), an efficient symmetric normalization technique is introduced. Extensive experiments on ImageNet, COCO and ADE20K show that our SOFT significantly improves the computational efficiency of existing ViT variants. With linear complexity, much longer token sequences are permitted by SOFT, resulting in superior trade-off between accuracy and complexity. Code and models are available at <https://github.com/fudan-zvg/SOFT>.

Keywords Transformer · linear complexity · softmax normalization · softmax-free · Gaussian attention

1 Introduction

Recently the step change brought by Transformers (Vaswani et al., 2017) in natural language processing (NLP) (Brown et al., 2020, Devlin et al., 2019) seems to have arrived in vision (Dosovitskiy et al., 2021, Yuan et al., 2021, Zheng et al., 2021, Zhu et al., 2021). Indeed, with less inductive bias in its architecture design than Convolution neural networks (CNNs), pure Vision Transformer (ViT) (Dosovitskiy et al., 2021) and its variants have shown to be able to outperform CNNs on various vision tasks (d’Ascoli et al., 2021, Jaegle et al., 2021). However, there is a bottleneck in any Transformer based model, namely its quadratic complexity in both computation and memory usage. This is intrinsic to the self-attention mechanism: given a sequence of tokens (*e.g.*, words or image patches) as input, the self-attention module iteratively learns the feature representations by relating one token to all other tokens. This results in a quadratic complexity $O(n^2)$ with the token sequence length n in both computation (time) and memory (space) since an $n \times n$ sized attention matrix needs to be computed and saved during inference. This problem is particularly acute in vision: a 2D image after tokenization will produce a far longer sequence than those in NLP even with a moderate spatial resolution. This quadratic complexity thus prevents a ViT model from modeling images at high spatial resolutions, which are often crucial for visual recognition tasks.

A natural solution is to reduce the complexity of self-attention computation via approximation. Indeed, there have been a number of attempts in NLP (Choromanski et al., 2021, Kitaev et al., 2020, Wang et al., 2020, Xiong et al., 2021). For example, (Wang et al.,

Corresponding author: Li Zhang
E-mail: lizhangfd@fudan.edu.cn

¹ School of Data Science, Fudan University, Shanghai, China

² University of Surrey, Guildford, UK

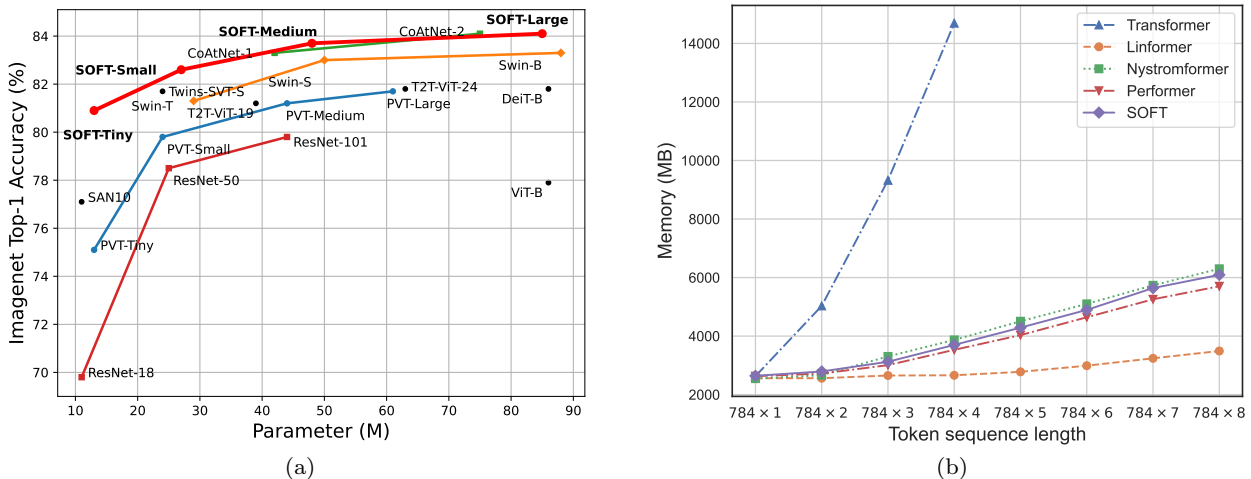


Fig. 1 Top-1 classification accuracy on ImageNet (Deng et al., 2009) validation set with respect to parameters and the memory usage corresponding to the token sequence length in practice compared to other methods. (a) Comparison with CNN models: ResNet (He et al., 2016) and CoAtNet (Dai et al., 2021) Transformer models: PVT (Wang et al., 2021), Swin (Liu et al., 2021), DeiT (Touvron et al., 2021a), ViT (Dosovitskiy et al., 2021), T2T-ViT (Yuan et al., 2021), Twins-SVT (Chu et al., 2021) and SAN10 (Zhao et al., 2020); (b) Comparison with Transformer (Vaswani et al., 2017), Linformer (Wang et al., 2020), Nyströformer (Xiong et al., 2021) and Performer (Choromanski et al., 2021). The memory usage is measured with a batch size of 1 on a 16GB Tesla V100.

2020) takes a naive approach by shortening the length of Key and Value via learnable projections. Such a coarse approximation would inevitably cause performance degradation. In contrast, (Choromanski et al., 2021, Katharopoulos et al., 2020) both leverage the kernel mechanism to approximate softmax normalization to linearize the computation in self-attention. (Kitaev et al., 2020) instead adopts a hashing strategy to selectively compute the most similar pairs. Recently, (Xiong et al., 2021) uses Nyström matrix decomposition to reconstruct the full attention matrix with polynomial iteration for approximating the pseudo-inverse of the landmark matrix. Nonetheless, softmax normalization is simply duplicated across the matrix decomposition process, which is theoretically unsound. We empirically found that none of these methods are effective when applied to vision (see Sec. 4.1).

In this work, we identify that the limitations of existing efficient Transformers are caused by the use of *softmax self-attention*, and for the first time propose a softmax-free Transformer. More specifically, in all existing Transformers (with or without linearization), a softmax normalization is needed on top of scaled dot-product between token feature vectors (Vaswani et al., 2017). Keeping this softmax operation challenges any subsequent linearization efforts. To overcome this obstacle, we introduce a novel *softmax-free self-attention* mechanism, named as SOFT, with linear complexity $O(n)$ in both space and time. Specifically, SOFT uses Gaussian kernel to define the similarity (self-attention)

function without the need for subsequent softmax normalization. With this softmax-free attention matrix, we further introduce a novel low-rank matrix decomposition algorithm for approximation. The robustness of the approximation is theoretically guaranteed by employing a Newton-Raphson method for reliably computing the Moore-Penrose inverse of the matrix.

We make the following **contributions**. **(I)** We introduce a novel *softmax-free Transformer* with linear space and time complexity. **(II)** Our attention matrix approximation is achieved through a novel matrix decomposition algorithm with theoretical guarantee. **(III)** To evaluate our method for visual recognition tasks, we design a family of generic backbone architectures with varying capacities using SOFT as the core self-attention component. Extensive experiments show that with a linear complexity (Figure 1b), our SOFT models can take in as input much longer image token sequences. As a result, with the same model size, our SOFT outperforms the state-of-the-art CNNs and ViT variants on ImageNet (Deng et al., 2009) classification in the accuracy/complexity trade-off (Figure 1a).

A preliminary version of this work was presented in NeurIPS 2021 spotlight (Lu et al., 2021). In this paper, we have further extended our conference version as follows: (i) We improve the efficiency and robustness in computing Moore-Penrose inverse by using an iterative method in the forward process only while calculating its theoretical gradient only once in the backward propagation. (ii) We analyze the limita-

tions of our preliminary SOFT from a matrix spectral norm perspective, revealing the importance of normalization for enhancing the model’s task generalizability. (iii) We prove that the preliminary SOFT experiences a second-order increase in matrix spectral norm relative to the matrix size, making it fail in dense vision problems. (iv) To address these limitations, we propose a normalized softmax-free self-attention, keeping linear complexity while enhancing performance, supported by both theoretical proof and extensive experiments. (v) The improved SOFT outperforms the state-of-the-art CNNs and ViTs for classification on ImageNet (Deng et al., 2009), object detection on COCO (Lin et al., 2014) and semantic segmentation on ADE20K (Zhou et al., 2019).

2 Related work

2.1 Vision Transformers

There is a surge of research interests recently in exploiting Transformers for visual recognition tasks (Guo et al., 2022, Touvron et al., 2021a, Wang et al., 2021, 2018, Yuan et al., 2021, Zhang et al., 2020), inspired by their remarkable success in NLP (Brown et al., 2020, Devlin et al., 2019, Vaswani et al., 2017). Core to these NLP and vision transformers is the same self-attention mechanism (Vaswani et al., 2017) that computes a self-attention matrix by exhaustively comparing token pairs. This means a quadratic complexity with the sequence length in both space and time, which thus limits the scalability of Transformers in dealing with long sequences. This limitation is more serious in vision than NLP: To process an image with at least thousands of pixels, patch-wise tokenization is a must for Transformers to control the computational cost. Given higher resolution images, the patch size also needs to be enlarged proportionally sacrificing the spatial resolution. This limits the capability of Transformers, *e.g.*, learning fine-grained feature representation as required in many visual recognition tasks.

2.2 Linear Transformers

Recently, there have been a number of linear/efficient variants (Choromanski et al., 2021, Kasai et al., 2021, Katharopoulos et al., 2020, Kitaev et al., 2020, Peng et al., 2021, Tay et al., 2023, Wang et al., 2020) of Transformers in NLP. For example, (Wang et al., 2020) learns to shrink the length of Key and Value based on a low-rank assumption. (Kitaev et al., 2020) adopts

a hashing strategy to selective the most similar pairs and only compute attention among them. (Choromanski et al., 2021, Katharopoulos et al., 2020) utilize different kernel functions for approximating softmax-based self-attention matrix. (Peng et al., 2021) applies random feature mapping on the sequences to approach the original softmax function. (Kasai et al., 2021) decreases the time and memory consumption of the attention matrix by replacing the softmax function with its linear-complexity recurrent alternative. When applied to visual recognition tasks, however, we show that these models have considerable performance degradation compared to the standard Transformers (Vaswani et al., 2017) (see Sec. 4.1).

The most related work to SOFT is (Xiong et al., 2021) which uses the Nyström matrix decomposition to avoid computing the full attention matrix. However, this method suffers from several theoretical defects: (1) As the standard self-attention needs to apply row-wise softmax normalization on the full attention matrix, a direct application of matrix decomposition is infeasible. As a workaround without solid theoretical support, softmax is simply applied to all the ingredient matrices in (Xiong et al., 2021). Such an approximation is not guaranteed theoretically. (2) With a polynomial iteration method, it is not guaranteed that the generalized attention matrix inverse can be computed when the matrix is a nearly singular one in practice. In contrast to all the above methods, in this paper we propose a *softmax-free* self-attention mechanism that facilitates matrix decomposition for complexity minimization with theoretical guarantees.

3 Method

3.1 Softmax-free self-attention formulation

A schematic illustration of our model is given in Figure 2. Let’s first look at our attention module design. Given a sequence of n tokens $X \in \mathbb{R}^{n \times d}$ with each token represented by a d -dimensional feature vector, self-attention (Vaswani et al., 2017) aims to discover the correlations of all token pairs exhaustively.

Formally, X is first linearly projected into three d_e -dimensional spaces (**query**, **key**, and **values**) as:

$$Q = XW_q \in \mathbb{R}^{n \times d_e}, K = XW_k \in \mathbb{R}^{n \times d_e}, V = XW_v \in \mathbb{R}^{n \times d_e}, \quad (1)$$

where $W_q, W_k, W_v \in \mathbb{R}^{d \times d_e}$ are learnable matrices. For equation simplicity, we omit the multi-head notation in self-attention operations. However, it should be noted

that multi-head mechanisms are employed throughout. Self-attention can be expressed in a generic formulation as:

$$y_{i,:} = \sum_{j=1}^n \alpha(Q_{i,:}, K_{j,:}) \odot V_{j,:}, \quad (2)$$

where \odot is the Hadamard product, and $i, j \in \{1, \dots, n\}$ index the tokens. The key self-attention function $\alpha : \mathbb{R}^{d_e} \times \mathbb{R}^{d_e} \rightarrow \mathbb{R}$ is composed of a nonlinear function $\beta : \mathbb{R} \rightarrow \mathbb{R}$ and a relation function $\gamma : \mathbb{R}^{d_e} \times \mathbb{R}^{d_e} \rightarrow \mathbb{R}$. A dominant instantiation of α is the scaled dot-product based softmax self-attention (Vaswani et al., 2017), defined as

$$\beta(\cdot) = \text{softmax}(\cdot), \quad \gamma(Q_{i,:}, K_{j,:}) = \frac{1}{\sqrt{d_e}} \cdot Q_{i,:}^\top K_{j,:}. \quad (3)$$

Whilst this softmax self-attention has been the *de facto* choice and seldomly questioned, as discussed earlier it is not necessarily suited for linearization. To facilitate the design of linear self-attention, we introduce a softmax-free self-attention function with the dot-product replaced by a Gaussian kernel as:

$$\beta'(\cdot) = \exp(\cdot), \quad \gamma'(Q_{i,:}, K_{j,:}) = -\frac{1}{2\sqrt{d_e}} \cdot \|Q_{i,:} - K_{j,:}\|_2^2. \quad (4)$$

A dissection of Transformers by Tsai et al. (Tsai et al., 2019) reveals negligible performance differences between asymmetric and symmetric kernels. To maintain the symmetric properties of the attention matrix as defined in Eq. (3), we opt for identical projection matrices W_q and W_k in Eq. (1), effectively setting $Q = K$. To further investigate the impact of symmetric kernels, additional experiments are conducted in our ablation studies of Section 4.4. Our self-attention matrix is then written as:

$$S_{i,j} = \exp\left(-\frac{1}{2\sqrt{d_e}} \cdot \|Q_{i,:} - K_{j,:}\|_2^2\right). \quad (5)$$

For notation simplicity, we define the matrix formulation as: $S = \exp(Q \ominus K)$.

Remarks: Our self-attention matrix S has three important properties: (1) It is symmetric; (2) All the elements lie in a unit range of $[0, 1]$; (3) All diagonal elements hold the largest value 1 (self-reinforced), with the bottom ones (corresponding to most dissimilar token pairs) being close to 0. As Gaussian kernel is a positive definite kernel (Fasshauer, 2011), S is deemed a Gram matrix. However, we find that when using our kernel-based self-attention matrix S without linearization, the training of a transformer fails to converge. More discussion can be found in Section 3.3.

3.2 Low-rank regularization via matrix decomposition with linear complexity

To solve the convergence and quadratic complexity problems, we leverage matrix decomposition as a unified solution with low-rank regularization. In particular, we consider Nyström (Williams and Seeger, 2000), which is originally a low-rank matrix approximation algorithm. This enables our model’s complexity to be reduced significantly without computing the full self-attention matrix S .

We make this choice because our S is positive semi-definite (*i.e.*, a Gram matrix) without follow-up normalization which are all necessary conditions for Nyström. In contrast, (Xiong et al., 2021) totally ignores these requirements, leading to theoretical flaw in its approximation.

To define the Nyström method formally, let us express $S = \exp(Q \ominus K)$ as a block matrix:

$$S = \begin{bmatrix} A & B \\ B^\top & C \end{bmatrix} \in \mathbb{R}^{n \times n}, \quad (6)$$

where $A \in \mathbb{R}^{m \times m}$, $B \in \mathbb{R}^{m \times (n-m)}$, $C \in \mathbb{R}^{(n-m) \times (n-m)}$ with $m \ll n$. Through Nyström decomposition (see derivative details in Appendix A), an approximation can be represented as:

$$\hat{S} = \begin{bmatrix} A \\ B^\top \end{bmatrix} A^\dagger [A \ B] = P^\top A^\dagger P, \quad \text{where } P = [A \ B], \quad (7)$$

and A^\dagger is the Moore-Penrose (a generalized) inverse of A .

Algorithm 1: SOFT: Softmax-free attention

Input: $Q \in \mathbb{R}^{n \times d_e}$, sampling function f_s

Sampling $\tilde{Q} \leftarrow f_s(Q)$;

$A \leftarrow \exp(\tilde{Q} \ominus \tilde{Q})$, $P \leftarrow \exp(\tilde{Q} \ominus Q)$;

$\hat{S} \leftarrow P^\top \text{NR}(A)P$;

Output: \hat{S}

Algorithm 2: NR: Newton-Raphson iteration

Input: $A \in \mathbb{R}^{m \times m}$, and $\mathcal{T} \in \mathbb{Z}^+$

$\alpha = 2/\|A\|_1^2$. Initialize $A_0 \leftarrow \alpha A$;

for k from 1 to \mathcal{T} **do**

$A_k \leftarrow 2A_{k-1} - A_{k-1}AA_{k-1}$

end

Output: $A_{\mathcal{T}}$

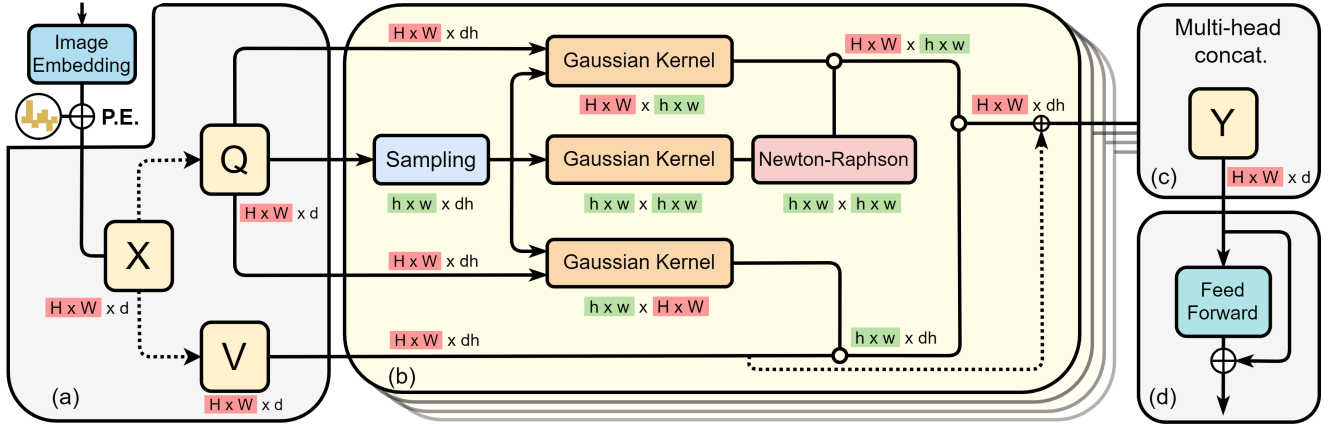


Fig. 2 Schematic illustration of the proposed *softmax-free self-attention* (SOFT) method. P.E.: Position embedding. Dash lines: linear projection. dh : the hidden dim of each attention head. \circ denotes the matrix dot product.

Sampling: In the standard Nyström formulation, A and B are sub-matrices of S obtained by randomly sampled m tokens, denoted as \tilde{Q} . We call the sampled \tilde{Q} as *bottleneck tokens*. However, we find empirically that random sampling is considerably sensitive to the choice of m . We hence explore two additional options to leverage the structural prior of visual data: (1) Using one convolutional layer with kernel size k and stride k to learn \tilde{Q} , and (2) Using average pooling with kernel size k and stride k to generate \tilde{Q} . For both, we need to reshape Q to the form of $\mathbb{R}^{H \times W \times d_e}$. Each slide of convolution or pooling produces a token. We set k according to the length of Q such that m tokens can be obtained. Our experiments show that a convolution layer performs better in accuracy. We therefore use a convolution layer by default.

As K is identical to Q , we have $\tilde{K} = \tilde{Q}$. Given these m tokens, we then compute *bottleneck attention* A and P as:

$$A = \exp(\tilde{Q} \ominus \tilde{K}), \quad P = \exp(\tilde{Q} \ominus K). \quad (8)$$

We finally obtain a regularized self-attention matrix \hat{S} of SOFT as:

$$\hat{S} = \exp(Q \ominus \tilde{K}) \left(\exp(\tilde{Q} \ominus \tilde{K}) \right)^\dagger \exp(\tilde{Q} \ominus K). \quad (9)$$

The overall SOFT is summarized in Algorithm 1. The *low-rank* regularization is conducted as follows. For computing the attention score between any two tokens, we first correlate each of them with sampled tokens using our self-attention function (Equation (5)); With this correlation representation we then compute their similarity under the modulation of the generalized inverse of \tilde{Q} 's correlation matrix. Similar as the standard Nyström, our design associates the input tokens w.r.t. a

small space spanned by a set of sampled tokens, giving a proper estimation of the original attention relationships subject to a low-rank constraint. This method is proved in Appendix A.

Moore-Penrose inverse: An accurate and commonly used way to calculate the Moore-Penrose inverse is to use Singular Value Decomposition (SVD). Given $A \in \mathbb{R}^{m \times m}$ and its SVD form $A = U \Sigma V^\top$ where U, V are $m \times m$ unitary matrices and Σ is a $m \times m$ diagonal matrix, the Moore-Penrose inverse of A is $A^\dagger = V \Sigma^\dagger U^\top$. Nevertheless, SVD is not friendly to the training process on GPU hence harming the model training efficiency. To solve this issue, we adopt the Newton-Raphson method. It is an iterative algorithm with the $(k+1)$ -th iteration formulated given the previous iteration as:

$$A_{k+1} = 2A_k - A_k A A_k, \quad \text{and} \quad A_0 = \alpha A. \quad (10)$$

We now prove that A_k finally converges to Moore-Penrose inverse of $A_{m \times m}$, if α is sufficiently small (Ben-Israel and Cohen, 1966).

Proposition 1 *When α is sufficiently small, $A_{k+1} = 2A_k - A_k A A_k$, A_k converges to A^\dagger .*

The proposition is proved in Appendix B. Though $\alpha = 2/\|A\|_1^2$ which ensures good convergence behavior in Algorithm 2, in practice, we find that using an alternative form gives more stable training and faster convergence. Specifically, in $\|I - A \frac{2\beta^n}{\|A\|_1^2}\|_1 \leq 1$ where β equals to 0.5, we find the smallest n_i that holds this inequality. Then, we initialize α as $\alpha = \frac{2\beta^{n_i}}{\|A\|_1^2}$.

The following proposition comes with the proof of Proposition 1:

Proposition 2 *$\|A A_k A - A\|$ and $\|A_k - A^\dagger\|$ decreases to 0 monotonously, if α is sufficiently small.*

Proof Note that when we multiply A on both sides of (33), the equation turns to be:

$$\begin{aligned} A - AA_{k+1}A &= A(A^\dagger - A_k)A(A^\dagger - A_k)A \\ &= (AA^\dagger - AA_k)(A - AA_kA). \end{aligned} \quad (11)$$

Similarly norm both sides of (11), considering that $\|AA^\dagger - AA_k\| \rightarrow 0$ and $\|AA^\dagger - AA_k\| < 1$ always holds, $\|A - AA_kA\|$ monotonically decreases to 0. The inequality (34) implies that $\|A_k - A^\dagger\|$ decreases to 0 monotonously.

Note although $\|A - AA_kA\|$ monotonically decreases to 0, $\|A_kAA_k - A_k\|$ cannot be proved to be so yet.

This ensures that our estimated inverse is sufficiently accurate for matrix decomposition, subject to that our SOFT attention is regularized. In training stage, we find that bottleneck matrix A is always non-singular in practice and its inverse A^{-1} thus exists. Therefore, the iteration can be avoided in back propagation because the differential of matrix inverse can be explicitly expressed as

$$\nabla_x \mathcal{L} = -Y^\top (\nabla_Y \mathcal{L}) Y^\top, \quad (12)$$

where $X \in \mathbb{R}^{m \times m}$ is a non-singular matrix and Y is the inverse of X , i.e., $Y = X^{-1}$, $\nabla_Y \mathcal{L}$ is the gradient of loss \mathcal{L} on Y and $\nabla_X \mathcal{L}$ is the gradient of loss \mathcal{L} on X . This can accelerate the training, as validated in Sec. 4.1. The theoretical proof is shown in Appendix B.

Complexity: We summarize the complexity of SOFT in space and time. For *time complexity*, it involves: (1) Sampling: $\mathcal{O}(nd_e)$. (2) Calculating three decomposed matrices: $\mathcal{O}(nmd_e + mnd_e + m^2d_e) = \mathcal{O}(2mnd_e + m^2d_e)$; (3) Moore-Penrose inverse: $\mathcal{O}(\mathcal{T} \times m^3) = \mathcal{O}(\mathcal{T}m^3)$, where \mathcal{T} is the iteration steps. (4) All matrix multiplication: $\mathcal{O}(nm^2 + mnd_e + mnd_e) = \mathcal{O}(nm^2 + 2mnd_e)$. The total time complexity is $\mathcal{O}((d_e + 4md_e + m^2)n + \mathcal{T}m^3 + d_em^2)$. The *space complexity* is decided by four decomposed matrices with $\mathcal{O}(n \times m) + \mathcal{O}(m \times m) + \mathcal{O}(m \times n) + \mathcal{O}(n \times d_e) = \mathcal{O}((2m + d_e)n + m^2)$. As we keep m ($m \ll n$) a fixed constant in our model, both time and space complexity are $\mathcal{O}(n)$, making SOFT a linear self-attention.

3.3 Attention normalization

Whilst the above SOFT formulation is competitive for image classification, transferring the pre-trained model to downstream tasks with different input token sequence lengths is limited. We conduct analysis on the model's sensitivity against input perturbation. As suggested in (Yoshida and Miyato, 2017), all parts of a model should have small *spectral norm* (i.e., matrix 2-norm or the

largest singular value of a matrix). Concretely, by the triangle inequality $\|XY\|_2 \leq \|X\|_2\|Y\|_2$ where X and Y are any real matrix, any part with large spectral norm could lead to significant error accumulation. This also applies for self-attention matrix, since it is often symmetric and non-negative definite and its spectral norm corresponds to the largest eigenvalue. We provide more theoretical analysis below. Note that both scale dot-product kernel (linear kernel) and Gaussian kernel are positive definite kernels, so they have non-negative eigenvalues.

Proposition 3 *In scaled dot-product based softmax self-attention, assume $\lambda_1 \geq \lambda_2 \geq \dots \lambda_n \geq 0$ are eigenvalues of self-attention matrix $S_{softmax} \in \mathbb{R}^{n \times n}$, then $\lambda_1 \leq 1$.*

Proof We rewrite the softmax self-attention as

$$S_{softmax} = D^{-1}A, \quad (13)$$

where $A \in \mathbb{R}^{n \times n}$ is a real symmetric matrix, and $D = \text{diag}(A\mathbb{1}_n)$. We consider the graph Laplacian L of matrix A defined by $L = D - A$, then the normalized graph Laplacian can be expressed as

$$L_{rw} = D^{-1}L = D^{-1}(D - A) = I - D^{-1}A, \quad (14)$$

where, I is an identity matrix. According to (Von Luxburg, 2007), L_{rw} is a real semi-definite matrix, so all the eigenvalue of L_{rw} is non-negative. Therefore, eigenvalues of $I - D^{-1}A$ are non-negative, which leads to the fact that eigenvalues $\lambda_1, \dots, \lambda_n$ of $D^{-1}A$ is less or equal to 1.

This proposition means that softmax normalization is useful in restricting the range of self-attention matrix's eigenvalues to $[0, 1]$ and eventually the effect of error accumulation. This is an important role *softmax* operation plays in improving generalizability with standard self-attention. However, this is not the case for our softmax-free self-attention as formulated above.

Proposition 4 *In Gaussian kernel-based self-attention, if $\lambda_1 \geq \lambda_2 \geq \dots \lambda_n \geq 0$ are eigenvalues of self-attention matrix $S_{gaussian} \in \mathbb{R}^{n \times n}$, then $\lambda_1 \leq n$.*

Proof

$$\sum_{i=1}^n \lambda_i = \text{Tr}(A) = n,$$

since the diagonal elements of Gaussian kernel-based self-attention is always 1. Therefore, with the fact that all the eigenvalues are positive, we have $\lambda_1 \leq n$.

A larger upper bound of eigenvalue with our proposed self-attention could thus lead to less generalizability, due to a trend of higher error accumulation. Specifically, for a softmax-free self-attention matrix, $\hat{S} = P^\top A^\dagger P$, we have

$$\|\hat{S}\|_2 = \|P^\top A^\dagger P\|_2 \leq \|P\|_2^2 \|A^\dagger\|_2. \quad (15)$$

For the bottleneck matrix of softmax-free attention $A \in \mathbb{R}^{m \times m}$, we assume it is k -connected ($k \ll m$), *i.e.*, there are k fields disconnected with each other. This is because a field represents a semantic part of an image and the number is often small.

Proposition 5 *Assume the bottleneck matrix of softmax-free attention, $A \in \mathbb{R}^{m \times m}$ is k -connected. If $\lambda_1 \geq \lambda_2 \geq \dots \geq \lambda_m \geq 0$ are eigenvalues of A^\dagger , then $\lambda_1 = \mathcal{O}(m^2)$ and $\|A^\dagger\|_2 = \mathcal{O}(m^2)$.*

The proposition is proved in Appendix C. This proposition indicates that $\|\hat{S}\|_2$ is proportional quadratically with the length m of bottleneck token sequence. It implies that the above SOFT formula would be limited to the applications with short bottleneck token sequences (*e.g.*, image classification).

Proposition 6 *For the bottleneck matrix of SOFT self-attention $A \in \mathbb{R}^{m \times m}$, we have*

$$\|D^{-1/2} A^\dagger D^{-1/2}\|_2 = \mathcal{O}(m), \quad (16)$$

where $D = \text{diag}(A \mathbb{1}_m)$ and $\mathbb{1}_m$ is an all one m -D vector.

Proof

$$\|D^{-1/2} A^\dagger D^{-1/2}\|_2 \leq \|D^{-1/2}\|_2^2 \|A^\dagger\|_2 = \|D^{-1}\|_2 \|A^\dagger\|_2,$$

also, D is a diagonal matrix,

$$\|D^{-1}\|_2 \|A^\dagger\|_2 = \|D^{-1} A^\dagger\|_2 = \|A_n^\dagger\|_2 = \mathcal{O}(m)$$

This proposition suggests that symmetric normalization can lower the largest eigenvalue of A^\dagger , reducing the spectral norm of \hat{S} .

Attention normalization: In light of the above theorem, we further introduce the normalization of SOFT as:

$$\hat{S} = \exp(Q \ominus \tilde{K}) D^{-\frac{1}{2}} \left(\exp(\tilde{Q} \ominus \tilde{K}) \right)^\dagger D^{-\frac{1}{2}} \exp(\tilde{Q} \ominus K) \quad (17)$$

where $D = \text{diag}(\exp(\tilde{Q} \ominus \tilde{K}) \mathbb{1}_m)$. This yields a tiny increase of $\mathcal{O}(m^2)$ in the computational complexity, which can be further reduced to $\mathcal{O}(\log m)$ on GPU by parallel

reduction algorithm (Cheng et al., 2014). This discovery unleashes new possibilities for SOFT and paves the way for its expanded usage, particularly in applications that demand dense information reasoning (such as object detection and semantic segmentation). This results in our SOFT++ formulation.

3.4 Instantiations

Figure 2 shows how our proposed *softmax-free self-attention* block (**SOFT block**) can be implemented in a neural network. We replace the self-attention block with our SOFT block in the traditional Transformer, that is, we stack a SOFT block with a feed forward residual block (Dosovitskiy et al., 2021) to form a *softmax-free Transformer* layer (**SOFT layer**).

Focusing on the general image recognition tasks, we integrate our SOFT layer into the recent pyramidal Transformer architecture (Wang et al., 2021) to form our final model **SOFT**. Further, several improvements are introduced in patch embedding (*i.e.*, tokenization). Specifically, unlike (Wang et al., 2021) that uses a combination of non-overlapping convolution and layer normalization (Ba et al., 2016), we adopt a stack of overlapping convolutions, batch normalization (Ioffe and Szegedy, 2015) and ReLU non-linearity. Concretely, the STEM is implemented by 3 units of $3 \times 3 \text{ Conv} \rightarrow \text{BN} \rightarrow \text{ReLU}$, with the stride of 2, 1, 2 respectively. Then, one such unit is applied to each of three following down-sampling operations with stride of 2 in the multi-stage architecture.

The architecture hyper-parameters of SOFT are: d : the input channel dimension of SOFT layer. d_e : the embedding dimension of tokens in SOFT block. In practice, we set $d_e = d$. h : the head number of SOFT block. d_h : the channel dimension of each head and $d_h = d_e/h$. n : the input token sequence length of a SOFT block. m : the bottleneck token sequence length of SOFT block. sp : the sampling ratio of token sequence length sampling, which is the ratio between input token sequence length and the bottleneck token sequence length. e : the expansion ratio of the 2-layer feed forward block. In SOFT, for all the stages we set $d_h = 32$, $e = 4$ and $m = 49$, sp varies in each stage according to the input token sequence length. Table 1 details the family of our SOFT configurations with varying capacities (depth and width).

Table 1 Architecture specifications of SOFT variants. *sp.*: sampling ratio. *-d*: the hidden dimension. *-h*: the number of heads in the self-attention block. *C33-BN-ReLU*: three 3x3 Conv-BN-ReLU, with the stride of 2, 1, 2 respectively. *C31-BN-ReLU*: one 3x3 Conv-BN-ReLU, with a stride of 2.

	Tiny	Small	Medium	Large
	C33-BN-ReLU, 64-d			
Stage 1	$\begin{bmatrix} \text{sp. } 8 \times 8, \\ 64\text{-d, } 2\text{-h} \end{bmatrix} \times 2$	$\begin{bmatrix} \text{sp. } 8 \times 8, \\ 96\text{-d, } 3\text{-h} \end{bmatrix} \times 2$	$\begin{bmatrix} \text{sp. } 8 \times 8, \\ 96\text{-d, } 3\text{-h} \end{bmatrix} \times 2$	$\begin{bmatrix} \text{sp. } 8 \times 8, \\ 128\text{-d, } 4\text{-h} \end{bmatrix} \times 2$
	C31-BN-ReLU, 128-d			
Stage 2	$\begin{bmatrix} \text{sp. } 4 \times 4, \\ 128\text{-d, } 4\text{-h} \end{bmatrix} \times 2$	$\begin{bmatrix} \text{sp. } 4 \times 4, \\ 192\text{-d, } 6\text{-h} \end{bmatrix} \times 2$	$\begin{bmatrix} \text{sp. } 4 \times 4, \\ 192\text{-d, } 6\text{-h} \end{bmatrix} \times 2$	$\begin{bmatrix} \text{sp. } 4 \times 4, \\ 256\text{-d, } 8\text{-h} \end{bmatrix} \times 2$
	C31-BN-ReLU, 256-d			
Stage 3	$\begin{bmatrix} \text{sp. } 2 \times 2, \\ 320\text{-d, } 10\text{-h} \end{bmatrix} \times 5$	$\begin{bmatrix} \text{sp. } 2 \times 2, \\ 384\text{-d, } 12\text{-h} \end{bmatrix} \times 5$	$\begin{bmatrix} \text{sp. } 2 \times 2, \\ 384\text{-d, } 12\text{-h} \end{bmatrix} \times 18$	$\begin{bmatrix} \text{sp. } 2 \times 2, \\ 512\text{-d, } 16\text{-h} \end{bmatrix} \times 18$
	C31-BN-ReLU, 512-d			
Stage 4 w. cls token	$\begin{bmatrix} \text{sp. } 1 \times 1, \\ 512\text{-d, } 16\text{-h} \end{bmatrix} \times 2$	$\begin{bmatrix} \text{sp. } 1 \times 1, \\ 768\text{-d, } 24\text{-h} \end{bmatrix} \times 2$	$\begin{bmatrix} \text{sp. } 1 \times 1, \\ 768\text{-d, } 24\text{-h} \end{bmatrix} \times 2$	$\begin{bmatrix} \text{sp. } 1 \times 1, \\ 1024\text{-d, } 32\text{-h} \end{bmatrix} \times 2$

Table 2 Comparison of different linear/efficient transformer variants on ImageNet (Deng et al., 2009), based on our multi-stage Tiny configuration (see Table 1). The memory usage is measured with the batch size of 1024 which is our standard training setting. Transformer is tested at a batch size of 256, which is the maximal number possible with the GPU resource at our disposal. Throughput is in format as Train throughput / inference throughput.

Methods	Memory	Params	FLOPs	Throughput (img/s)	Top-1 %
Transformer (Vaswani et al., 2017)	19.0GB†	13M	3.9G	1073 / 3240	80.0
Linformer (Wang et al., 2020)	11.7GB	13M	1.9G	2767 / 3779	78.2
Performer (Choromanski et al., 2021)	15.0GB	13M	2.2G	2037 / 3657	76.1
Nyströmformer (Xiong et al., 2021)	17.2GB	13M	2.0G	1891 / 3518	80.1
SOFT	15.8GB	13M	1.9G	1730 / 3436	80.9
SOFT++	15.8GB	13M	1.9G	1730 / 3436	80.9

4 Experiments

4.1 Image classification

Dataset: We evaluate the proposed SOFT and SOFT++ on the ILSVRC-2012 ImageNet-1K dataset (Deng et al., 2009) with 1.28M training images and 50K validation images from 1,000 classes. Following the common practice, we train a model on the training set and evaluate on the validation set.

Metrics: For model performance, the top-1 accuracy on a single crop is reported. To assess the cost-effectiveness, we also report the model size and floating point operations (*i.e.*, FLOPs).

Implementation details: We use the code base (Wightman, 2019) with the default setting to train and test all the models. Specifically, we use weight decay of 0.05 and 10 epochs of linear warm-up. We conduct 300 epochs training with an AdamW optimizer and decreasing learn-

ing rate with the cosine annealing schedule. During training, random flipping, mixup (Zhang et al., 2018) and cutmix (Yun et al., 2019) are adopted for data augmentation. Label smoothing (Szegedy et al., 2016) is used for loss calculation. All our variants are trained with a batch size of 1024 on 32G NVIDIA V100 GPUs. We also implement our method using the Mindspore (Mindspore, 2020).

Comparison with existing linear Transformers: We compare our method with three existing linear Transformer models: Linformer (Wang et al., 2020), Performer (Choromanski et al., 2021), Nyströmformer (Xiong et al., 2021) in terms of model complexity and accuracy.

Two experimental settings are adopted. Under the first setting, for all methods we use the same Tiny (Table 1) architecture for a fair comparison. That is, we replace the core self-attention block in SOFT/SOFT++ with each baseline’s own attention block with the rest of the architecture unchanged. Note that the *spatial re-*

Table 3 Evaluation results on ILSVRC-2012 ImageNet-1K (Deng et al., 2009) validation set. We report the results using the input size of 224x224 pixels center cropped from resized images with 256x256 pixels. M.S.Out. stands for whether the model is designed for multi-scale output. †: Corrected FLOPs by taking into account the cost of attention matrix multiplication overlooked in the origin paper.

Model	Style	Resolution	M.S. Out.?	Params	FLOPs	Top-1 %.
ResNet-18 (He et al., 2016)	Convolution	224 ²	✓	11M	1.9G	69.8
PVT-Tiny (Wang et al., 2021)	Transformers	224 ²	✓	13M	1.9G†	75.1
ConViT-Ti+ (d’Ascoli et al., 2021)	Transformers	224 ²	✗	10M	2.0G	76.7
Coat-Lite Mini (Xu et al., 2021)	Transformers	224 ²	✓	11M	2.0G	78.9
LambdaNets-50 (Bello, 2021)	Transformers	224 ²	✓	16M	-	78.9
ViP-Ti (Sun et al., 2021)	Transformers	224 ²	✓	13M	1.7G	79.0
SOFT-Tiny	SOFT	224 ²	✓	13M	1.9G	80.9
SOFT++-Tiny	SOFT++	224 ²	✓	13M	1.9G	80.9
ResNet-50 (He et al., 2016)	Convolution	224 ²	✓	25M	4.1G	78.5
PVT-Small (Wang et al., 2021)	Transformer	224 ²	✓	24M	4.0G†	79.8
Swin-T (Liu et al., 2021)	Transformer	224 ²	✓	29M	4.5G	81.3
Twins-SVT-S (Chu et al., 2021)	Hybrid	224 ²	✓	24M	3.7G	81.7
CoAtNet-0 (Dai et al., 2021)	Hybrid	224 ²	✓	25M	4.2G	81.6
DeiT III-S (Touvron et al., 2022)	Transformer	224 ²	✗	22M	4.6G	81.4
SwinV2-T (Liu et al., 2022a)	Transformer	256 ²	✓	29M	4.5G	81.7
ConvNext-T (Liu et al., 2022b)	Hybrid	224 ²	✓	29M	4.5G	82.1
SOFT-Small	SOFT	224 ²	✓	27M	4.5G	82.5
SOFT++-Small	SOFT++	224 ²	✓	27M	4.5G	82.6
ResNet-101 (He et al., 2016)	Convolution	224 ²	✓	44M	7.9G	79.8
PVT-Medium (Wang et al., 2021)	Transformer	224 ²	✓	44M	7.0G†	81.2
ViT-Small/16 (Dosovitskiy et al., 2021)	Transformer	224 ²	✗	48M	9.9G	80.8
Swin-S (Liu et al., 2021)	Transformer	224 ²	✓	50M	8.7G	83.0
ConvNext-S (Liu et al., 2022b)	Hybrid	224 ²	✓	50M	8.7G	83.1
CoAtNet-1 (Dai et al., 2021)	Transformer	224 ²	✓	42M	8.4G	83.3
SwinV2-S (Liu et al., 2022a)	Transformer	256 ²	✓	50M	8.7G	83.6
SOFT-Medium	SOFT	224 ²	✓	48M	8.7G	83.2
SOFT++-Medium	SOFT++	224 ²	✓	48M	8.7G	83.7
CaiT-S36(Touvron et al., 2021b)	Transformer	224 ²	✓	88M	13.9G	83.3
Swin-B(Liu et al., 2021)	Transformer	224 ²	✓	88M	15.4G	83.3
Twins-SVT-L (Chu et al., 2021)	Hybrid	224 ²	✓	99M	14.8G	83.3
DeiT III-B (Touvron et al., 2022)	Transformer	224 ²	✗	87M	15.5G	83.8
ConvNext-S (Liu et al., 2022b)	Hybrid	224 ²	✓	89M	15.4G	83.8
CoAtNet-2 (Dai et al., 2021)	Hybrid	224 ²	✓	75M	15.7G	84.1
SwinV2-B (Liu et al., 2022a)	Transformer	256 ²	✓	88M	15.4G	84.1
SOFT-Large	SOFT	224 ²	✓	85M	15.4G	83.6
SOFT++-Large	SOFT++	224 ²	✓	85M	15.4G	84.1

duction module of (Wang et al., 2021) is a special case of Linformer (Wang et al., 2020). We set the reduction ratio to be identical to ours. With the same uniform

sampling idea, we replace the 1D window averaging of Nyströmformer (Xiong et al., 2021) (for NLP tasks) with 2D average pooling (for images). The downsam-

Table 4 Object detection (RetinaNet (Lin et al., 2017)) results on COCO (Lin et al., 2014) val2007. We report the results by training 12 epoch (1×) schedule. #P stands for parameter size. AP^b represents bounding box AP. Note, SOFT cannot converge in training.

Backbone	RetinaNet 1×						
	#P	AP	AP ₅₀	AP ₇₅	AP _S	AP _M	AP _L
ResNet18 (He et al., 2016)	21M	31.8	49.6	33.6	16.3	34.3	43.2
PVT-Tiny (Wang et al., 2021)	23M	36.7	56.9	38.9	22.6	38.8	50.0
PVTv2-B1 (Wang et al., 2022)	23M	41.2	61.9	43.9	25.4	44.5	54.3
SOFT+-Tiny	23M	41.9	62.7	44.7	27.8	45.4	55.6
ResNet50 (He et al., 2016)	38M	36.3	55.3	38.6	19.3	40.0	48.8
PVT-Small (Wang et al., 2021)	34M	40.4	61.3	43.0	25.0	42.9	55.7
ViL-S (Zhang et al., 2021)	35M	41.6	62.5	44.1	24.9	44.6	56.2
Swin-T(Liu et al., 2021)	38M	41.7	61.2	43.2	26.0	44.3	54.5
SOFT+-Small	38M	43.7	64.9	46.8	28.7	47.4	57.6
ResNet101 (He et al., 2016)	57M	38.5	57.8	41.2	21.4	42.6	51.1
PVT-Medium (Wang et al., 2021)	54M	41.9	63.1	44.3	25.0	44.9	57.6
ViL-M (Zhang et al., 2021)	50M	42.9	64.0	45.4	27.0	46.1	57.2
Swin-S(Liu et al., 2021)	60M	43.0	63.8	45.7	27.1	46.9	57.2
SOFT+-Medium	59M	44.3	64.7	47.4	29.0	48.2	59.9
ResNeXt101 (Xie et al., 2017)	95M	41.0	60.9	44.0	23.9	45.2	54.0
PVT-Large (Wang et al., 2021)	71M	42.6	63.7	45.4	25.8	46.0	58.4
Swin-B (Liu et al., 2021)	98M	44.7	65.9	49.2	-	-	-
SOFT+-Large	98M	47.0	67.8	50.4	30.2	50.9	62.0

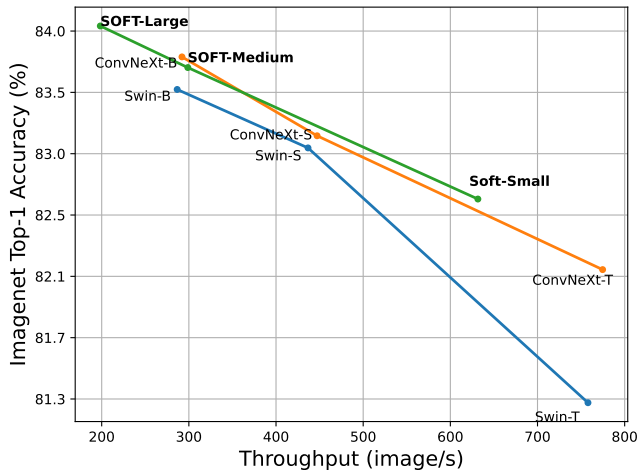


Fig. 3 A comparison of Top-1 classification accuracy on the ImageNet validation set (Deng et al., 2009) with respect to inference throughput for various models. Our comparison includes CNN models such as ConvNext (Liu et al., 2022b), as well as Transformer models like Swin (Liu et al., 2021). In this comparison, models positioned closer to the top-right indicate superior performance, balancing both accuracy and throughput effectively. Inference throughput is measured on a V100 GPU, following (Liu et al., 2021, 2022b).

pling ratio remains identical to ours. It is also worth mentioning that there is no official code released for Reformer (Kitaev et al., 2020) and the local Sensitive Hash (LSH) module has strict requirements on the length of input tokens. We thus do not include this method in our comparison.

From Table 3.4 we can make the following observations: (i) Linear Transformer methods substantially reduce the memory and FLOPs while maintain similar parameter size comparing to the Transformer on the Tiny architecture; (ii) Our approach SOFT/SOFT++ achieve the best classification accuracy among all the linearization methods. (iii) Our inference speed is on-par with other compared linear Transformers and our training speed is slightly slower than Nystromformer and both are slower than Performer and Linformer. Note that the slow training speed of our model is mostly due to the Newton-Raphson iteration which can only be applied sequentially for ensuring the accuracy of Moore-Penrose inverse. In summary, due to the on-par inference speed we consider the training cost increase is a price worth paying for our superior accuracy.

Under the second setting, we focus on the memory efficiency of SOFT against the baselines. Here we

Table 5 Instance segmentation (Mask R-CNN (He et al., 2017)) results on COCO (Lin et al., 2014) *val2007*. We report the results by training 12 epoch ($1\times$) schedule. #P stands for parameter size. AP^m represents mask AP respectively. Note, SOFT cannot converge in training.

Backbone	Mask R-CNN $1\times$						
	#P	AP^b	AP_{50}^b	AP_{75}^b	AP^m	AP_{50}^m	AP_{75}^m
ResNet18 (He et al., 2016)	31M	34.0	54.0	36.7	31.2	51.0	32.7
PVT-Tiny (Wang et al., 2021)	33M	36.7	59.2	39.3	35.1	56.7	37.3
PVTv2-B1 (Wang et al., 2022)	33M	41.8	64.3	45.9	38.8	61.2	41.6
SOFT++-Tiny	32M	41.2	63.7	44.7	38.2	61.0	41.0
ResNet50 (He et al., 2016)	44M	38.0	58.6	41.4	34.4	55.1	36.7
PVT-Small (Wang et al., 2021)	44M	40.4	62.9	43.8	37.8	60.1	40.3
ViL-S (Zhang et al., 2021)	45M	41.8	64.1	45.1	38.5	61.1	41.4
Swin-T(Liu et al., 2021)	48M	42.7	65.2	46.8	39.3	62.2	42.2
SOFT++-Small	48M	43.8	66.0	47.5	40.1	63.0	43.0
ResNet101 (He et al., 2016)	63M	40.4	61.1	44.2	36.4	57.7	38.8
PVT-Medium (Wang et al., 2021)	64M	42.0	64.4	45.6	39.0	61.6	42.1
ViL-M (Zhang et al., 2021)	60M	43.4	65.9	47.0	39.7	62.8	42.1
Swin-S(Liu et al., 2021)	69M	45.6	67.4	50.0	41.2	64.5	44.3
SOFT++-Medium	69M	46.6	67.8	51.2	42.0	64.8	45.2
ResNeXt101 (Xie et al., 2017)	101M	42.8	63.8	47.3	38.4	60.6	41.3
PVT-Large (Wang et al., 2021)	81M	42.9	65.0	46.6	39.5	61.9	42.5
Swin-B (Liu et al., 2021)	107M	45.5	-	-	41.3	-	-
SOFT++-Large	106M	47.0	68.3	51.7	42.2	65.2	45.4

follow the ViT (Dosovitskiy et al., 2021) network structure, stacking 12 attention layers with hidden dimension $d = 384$, heads $h = 12$, bottleneck token sequence length $m = 49$. Different attention blocks from the three linearized Transformer variants, Linformer (Wang et al., 2020), Performer (Choromanski et al., 2021), and Nyströmformer (Xiong et al., 2021) are studied. For each Transformer variant, we adjust its token sequence length n in a linear increment. Specifically, we use a token sequence length of $784 \times p$ where $p = 1, 2, 3, 4, 5, 6, 7, 8$ and set batch size 1 to verify whether the memory consumption increases “quadratically” or “linearly”. Figure 1b shows all compared transformer variants including our SOFT indeed have a linear memory usage complexity. This is in contrast with the standard Transformer which cannot cope with long token sequences with a quadratic complexity.

Comparison with state-of-the-art CNNs and ViTs:

We compare with state-of-the-art alternatives and report the top-1 accuracy on the ImageNet-1K validation set. FLOPs are calculated at batch size 1. From Figure 1a and Table 3, the following observations are made: (i) Overall, ViT and its variants yield better classification accuracy over CNNs. (ii) We achieve the best

performance among the recent pure vision Transformer based methods including ViT (Dosovitskiy et al., 2021) and DeiT (Touvron et al., 2021a), as well as the state-of-the-art CNN RegNet (Radosavovic et al., 2020). (iii) Our SOFT and SOFT++ outperform the most similar (in architecture configuration) Transformer counterparts PVT (Wang et al., 2021) at all variants. Since the attention module is the main difference, this validates directly the effectiveness of our model. (iv) We can also beat the latest ViT variants Twins (Chu et al., 2021) which is designed to address the efficiency limitation of ViT. We have done so with less parameters and fewer float point computation.

To gain insights into how attention is learned using our SOFT and the alternatives, Figure 4 shows the attention masks. For each model, we visualize the first two attention heads. It is evident that SOFT exhibits robustness and versatility in capturing local and long distance relations among pixels. We note that, although SOFT is trained for object categorization (ImageNet (Deng et al., 2009)), it seems to be able to learn both semantic concepts shared across instances in the same category and instance specific features. For instance, in the bottom-right example of a bird class, one attention

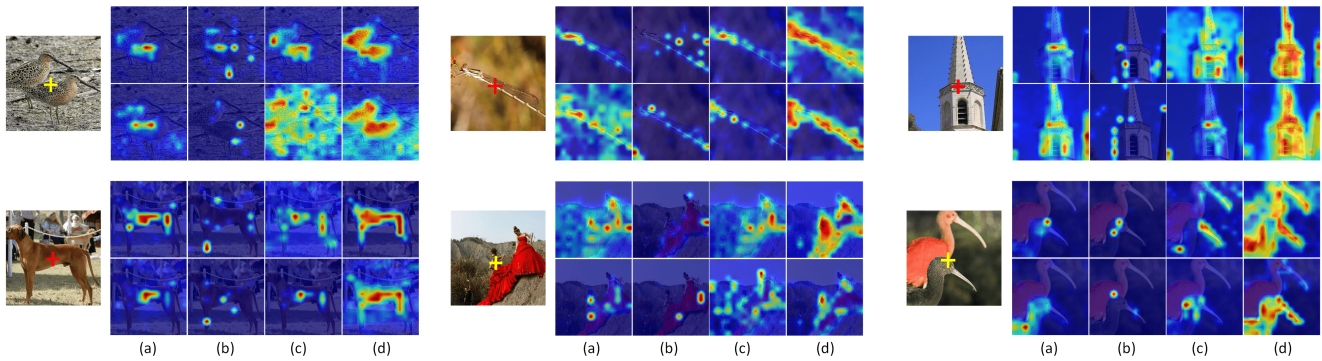


Fig. 4 Comparison of attention heatmaps for a selected query patch (indicated by a cross “+”) against all patches in an image. Heatmaps are derived from the first head’s corresponding row in the attention maps, as calculated by Equation 17. These heatmaps are normalized to a 0-1 scale, with warmer colors indicating higher relevance. The model variants compared are: (a) Transformer (Vaswani et al., 2017), (b) Performer (Choromanski et al., 2021), (c) Nystromformer (Xiong et al., 2021), and (d) Our SOFT approach. For additional examples, refer to Appendix E.

head focuses on the black bird only, while the other attends to both birds in the image. More examples are given in Appendix E.

Throughputs comparison: Figure 3 illustrates that our model achieves a superior balance between speed and performance compared to the Swin Transformer (Liu et al., 2021), and maintains a comparable balance with the current CNN state-of-the-art, ConvNext (Liu et al., 2022b). As detailed in Table 3.4, we employ a series-computed Newton iteration method to ensure numerical accuracy. While this approach slightly reduces speed, it preserves the accuracy of our model.

Comparison between SOFT and SOFT++ As shown in Table 3, SOFT++ performs equally well as SOFT for small models, and outperforms the preliminary version for larger models. Further, Table 6 validates the superiority of SOFT++ over SOFT in processing long token sequences in model deployment.

4.2 Object detection on COCO

Dataset: We evaluate the object detection performance of our SOFT++ on the COCO benchmark (Lin et al., 2014) including the `train2017` (118k images) and `val2017` (5k images) sets.

Implementation details: We consider two representative detectors: RetinaNet (Lin et al., 2017) and Mask R-CNN (He et al., 2017). We use AdamW optimizer with base learning rate of 1×10^{-4} and weight decay of 0.01. We train all the model with batch size 16 on 8 V100 GPUs. Following the practices of MMDetection (Chen et al., 2019), we adopt the $1\times$ and $3\times$ training schedules. In the training stage without multi-scale, images are resized to make the shorter sides at 800 pixels and the longer sides no exceeding 1333 pixels. In the train-

ing stage with multi-scale, the shorter sides of images are randomly resized to between 480 to 800.

Comparison with state-of-the-art CNNs and ViTs:

We compare with the state-of-the-art alternatives on RetinaNet (Lin et al., 2017) in Table 4 and Mask R-CNN (He et al., 2017) in Table 5. Our SOFT++ outperforms the CNN ResNet (He et al., 2016) and Transformer counterparts PVT (Wang et al., 2021) across all complexity groups in both object detection and instance segmentation, validating the superior trade-off between model complexity and performance by our design.

4.3 Semantic segmentation

Dataset: We evaluate the semantic segmentation performance of our SOFT++ on ADE20K (Zhou et al., 2019) and Cityscapes (Cordts et al., 2016).

Implementation details: UperNet (Xiao et al., 2018) is used as the framework. AdamW optimizer with 6×10^{-4} learning rate is applied to train ADE20K for 160k iterations and Cityscapes for 40k iterations. Images are cropped as 512×512 for ADE20K and 768×768 for Cityscapes during training. Multi-scale training and test time augmentation are not used.

Comparison with state-of-the-art CNNs and ViTs:

Table 7 shows that SOFT++ surpasses ResNet clearly, and the newest designed vision transformer Swin (Liu et al., 2021) and CovNext (Liu et al., 2022b) slightly under the similar parameters and float point computation cost.

4.4 Ablation studies

Pyramidal architecture: Unlike the earlier non-pyramidal vision Transformers (*e.g.*, ViT (Dosovitskiy et al., 2021)),

Table 6 The evaluation results on the validation set of ImageNet-1K (Deng et al., 2009) at various input sizes. The models were trained on the size of 224×224 . The down-sampling ratio of the patch embedding remains at 4.

Test input size	224×224	384×384	512×512
Token sequence length	3136	9216	16384
SOFT	82.5	33.7	0.14
SOFT++	82.6	82.6	80.2

Table 7 Semantic segmentation performance using our HLG Transformer with UperNet (Xiao et al., 2018) and SETR-PUP on Cityscapes validation set. Single-scale inference and 40k training schedules are used. Note, SOFT cannot converge in training.

Method	Backbone	#P	Cityscapes		ADE20K	
			FLOPs	mIoU	FLOPs	mIoU
FCN (Long et al., 2015)	ResNet-101	68M	619G	76.6	276G	39.9
PSPNet (Zhao et al., 2017)	ResNet-101	68M	576G	78.5	256G	44.4
DLabV3+ (Chen et al., 2018)	ResNet-101	62M	571G	79.3	262G	46.9
CCNet (Huang et al., 2019)	ResNet-101	68M	625G	80.2	278G	43.7
SETR (Zheng et al., 2021)	ViT-Large	318M	1340G	79.2	602G	48.5
OCRNet (Yuan et al., 2020)	HRNet-W48	70M	972G	81.1	164G	43.2
UperNet (Xiao et al., 2018)	Swin-T	60M	-	-	236G	44.5
UperNet (Xiao et al., 2018)	Swin-S	81M	-	-	259G	47.6
UperNet (Xiao et al., 2018)	Swin-B	121M	-	-	297G	48.1
UperNet (Xiao et al., 2018)	ConvNext	60M	-	-	235G	46.0
UperNet (Xiao et al., 2018)	ConvNext	82M	-	-	256G	48.7
UperNet (Xiao et al., 2018)	ConvNext	122M	-	-	293G	49.1
UperNet (Xiao et al., 2018)	SOFT++-Small	60M	545G	81.2	237G	46.5
UperNet (Xiao et al., 2018)	SOFT++-Med	81M	607G	82.0	260G	48.9
UperNet (Xiao et al., 2018)	SOFT++-Large	121M	899G	82.6	301G	49.2

most recent pyramidal (multi-scale) Transformers (*e.g.*, PVT (Wang et al., 2021)) use convolution layers to reduce the spatial resolution (*i.e.*, token sequence length) between stages. In this study, we ablate SOFT++ with a pyramidal architecture (our default SOFT++-Small), SOFT++ w/o a pyramidal architecture and DeiT-S (Touvron et al., 2021a) (no pyramidal architecture either). We replace the Transformer layer with a SOFT++ layer to get SOFT++ w/o a pyramidal architecture. Note all three variants have similar parameters and FLOPs. Table 11a shows that the conv-based pyramidal architecture is clearly superior to a non-pyramidal design, and our non-pyramidal counterpart is even slightly better than DeiT-S (Touvron et al., 2021a) whilst enjoying linear complexity.

Symmetric kernels: Tsai et al. (Tsai et al., 2019) conducted a comprehensive analysis of Transformers, revealing minimal performance disparities between asymmetric and symmetric kernels in NLP tasks, such as neural machine translation (NMT) and sequence pre-

diction (SP). In contrast, our research, detailed in Table 8, extends this investigation to the domain of computer vision, specifically focusing on image classification tasks. Our findings indicate that while symmetric kernels do have a marginal detrimental effect in computer vision tasks, this impact is relatively limited. Therefore, maintaining a symmetric kernel represents a balanced approach for enabling effective decomposition in our model.

Bottleneck token sequence length: In this study, we examine how the bottleneck token sequence length m , sampled from n tokens, influences the model’s performance. We change the bottleneck token sequence length in all stages to 36, 49, 64, 81. Table 9 shows that longer bottleneck token would increase the memory cost and the computational overhead. $m = 49$ seems to give the best trade-off between the performance and computational overhead. The memory usage is measured with the batch size of 128.

Table 8 Ablations on assessing the Impact of Symmetric Kernels on ImageNet-1K (Deng et al., 2009) image classification. As baselines for our study, we employ two of the most common backbones: ViT-small/16 (Dosovitskiy et al., 2021) and Swin-T (Liu et al., 2021).

Model	Asymmetric ($Q \neq K$)	Symmetric ($Q = K$)
ViT-Small/16 (Dosovitskiy et al., 2021)	80.8	80.5
Swin-T (Liu et al., 2021)	81.3	80.9

Table 9 Ablations on bottleneck token sequence length.

Bottleneck	Memory	FLOPs	Top-1 %
36	15.1GB	1.9G	80.5
49	15.8GB	1.9G	80.9
64	16.9GB	2.0G	80.9
81	18.5GB	2.1G	80.4

Table 10 Ablations on sampling methods.

Sampling methods	Params	FLOPs	Top-1 %
Convolution	13.07M	2.0G	80.9
Random sampling	12.96M	1.9G	80.8
Biased sampling	12.96M	1.9G	79.9
Average pooling	12.96M	1.9G	80.8

Table 11 (a) Ablations on pyramidal architecture. (b) Ablations on overlapped convolution.

Methods	Pyramidal?	Top-1 %	Methods	Overlapped?	Top-1 %
DeiT-S (Touvron et al., 2021a)	✗	79.8	PVT (Wang et al., 2021)	✗	75.1
SOFT++	✗	80.1	SOFT++	✗	78.4
SOFT++	✓	82.4	SOFT++	✓	80.9

Token sampling: The sampling function in SOFT++ can assume different forms. **Convolution:** The sequence $Q \in \mathbb{R}^{n \times d_e}$ is first reshaped to a feature map $\mathbb{R}^{H \times W \times d_e}$. $r \times r$ convolution kernel with stride of r is applied for downsampling, where $r = \sqrt{sp}$. The output channel size is also kept and no bias is used. At last, the feature map is reshaped back to the sequence. **Average pooling:** using a $r \times r$ kernel and r stride, where $r = \sqrt{sp}$. **Random sampling:** m tokens are randomly picked from n tokens. **Biased sampling:** We pick m tokens with a biased policy. Here, the first m tokens are picked. Table 10 shows that both convolution yields the best performance. Biased sampling can miss the most salient samples, and there is no guarantee that random sampling can keep the uniformity of the chosen samples. This result thus justifies the choice of using convolution in SOFT++.

Overlapped convolution: We ablate SOFT++ with overlapped convolution (our default choice, same as many

recent works) and with non-overlapped convolution in our Tiny configuration. Table 11b shows that overlapped convolution is a better choice. Our non-overlapped convolution variant still outperforms PVT (Wang et al., 2021) with the same non-overlapped convolution by a clear margin.

Newton-Raphson’s convergence: We study how many iterations the Newton-Raphson method needs to converge when computing the Moore-Penrose inverse A^\dagger . We use $\|AA_kA - A\|_p / \|A\|_p$ with $p = 2$ (see Proposition 2) as the convergence metric to quantify the difference between A_k and A^\dagger . Figure 5 shows that our approximation converges within 20 iterations across all stages.

Effect of attention normalization: Our attention normalization enables the model to perform more challenging vision tasks such as object detection and segmentation. This is because the leading eigenvalue of Gaussian kernel self-attention is conditioned on the token sequence length (Proposition 4), as shown in Figure

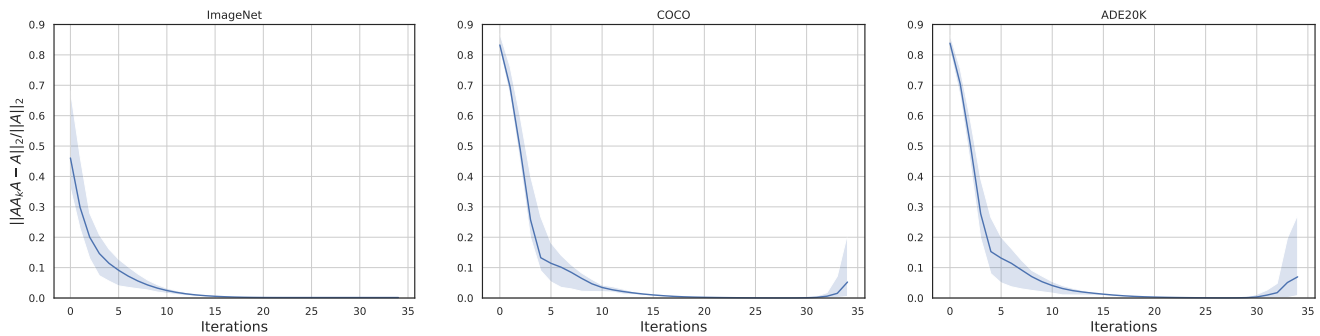


Fig. 5 Convergence analysis for the approximation of Moore-Penrose inverse on ImageNet, COCO and ADE20K separately. SOFT-Tiny is used. We measure $\|AA_kA - A\|_p / \|A\|_2$ for 100 input images on each dataset. The solid line shows the average convergence metric, while the shallow area indicates the upper bound and lower bound.

Table 12 Comparison of different linear/efficient Transformer variants on Long Range Arena (Tay et al., 2020), based on its official configuration. Our SOFT surpasses previous efficient methods on three tasks.

Methods	Listops(2K)	Text(4K)	Retrieval(4K)	Image(1K)	Avg. %
Transformer (Vaswani et al., 2017)	37.10	65.02	79.35	38.20	54.92
Reformer (Kitaev et al., 2020)	19.05	64.88	78.64	43.29	51.47
Linformer (Wang et al., 2020)	37.25	55.91	79.37	37.84	52.59
Performer (Choromanski et al., 2021)	18.80	63.81	78.62	37.07	49.58
Nyströmformer (Xiong et al., 2021)	37.15	65.52	79.56	41.58	55.95
SOFT	37.40	63.49	81.77	46.91	57.39

6a. And this effect can be clearly mitigated by our normalization scheme, as indicated in Figure 6b.

4.5 Additional experiments on NLP tasks

We compare our method with previous linear counterparts on four tasks of the Long Range Arena (LRA) (Tay et al., 2020) benchmark, including Listops (Nangia and Bowman, 2018), byte-level IMDb reviews text classification (Maas et al., 2011), byte-level document retrieval (Radev et al., 2013), and image classification on sequences of pixels (Krizhevsky, 2009).

Implementations. We use the Pytorch version of LRA (Tay et al., 2020) benchmark, provided by (Xiong et al., 2021). For the evaluation protocol, we strictly follow (Tay et al., 2020, Xiong et al., 2021). We omit the Pathfinder(1K) task as we cannot replicate the result of Nyströmformer (Xiong et al., 2021). For our SOFT, we simply use the average pooling with window size 4, stride 4 to sample the bottlenecks. We follow the configurations of (Xiong et al., 2021) with 2 layers, 64 and 128 hidden dimension respectively, and 2 attention heads. Table 12 shows that our SOFT outperforms both the

standard and alternative efficient Transformers on three out of four tasks, as well as the average performance.

5 Conclusions

In this work, we have introduced a novel softmax-free self-attention (SOFT) mechanism for linearizing Transformer’s complexity in space and time. Unlike existing linear Transformers that aim to approximate the conventional softmax based self-attention, SOFT employs a Gaussian kernel based attention which eliminates the need for softmax normalization. This design enables a full self-attention matrix to be approximated via low-rank matrix decomposition. The robustness of this proposed approximation is achieved by calculating its Moore-Penrose inverse using a Newton-Raphson method and an efficient symmetric attention normalization. Extensive experiments show that SOFT yields superior trade-off in accuracy and complexity on a variety of vision and language tasks.

Acknowledgements This work was supported in part by STI2030-Major Projects (Grant No. 2021ZD0200204), National Natural Science Foundation of China (Grant No. 62106050 and 62376060), Natural Science Foundation of Shanghai (Grant

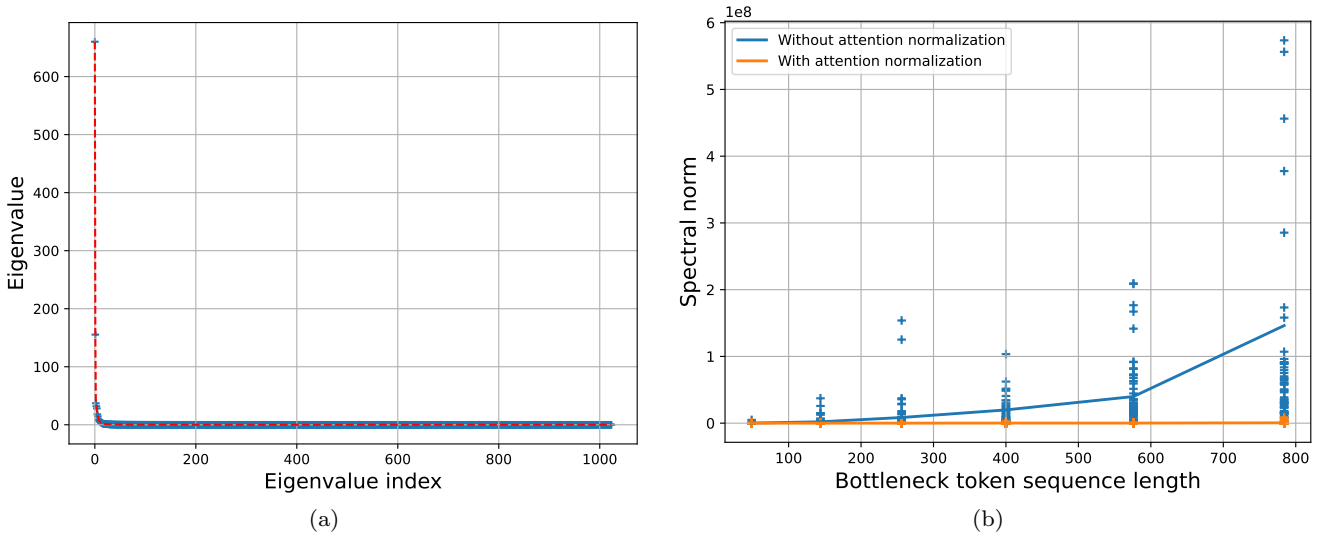


Fig. 6 (a) Eigenvalues of a specific bottleneck matrix $A \in \mathbb{R}^{1024 \times 1024}$. The auxiliary (red dash) line connects all the eigenvalues. (b) Comparing the spectral norm of self-attention matrix A^\dagger (without normalization, blue) and $D^{-1/2}A^\dagger D^{-1/2}$ (with normalization, orange) under a variety of bottleneck token sequence lengths. “+” represents individual samples; The lines connect the average norm at each token sequence length.

No. 22ZR1407500) and Lingang Laboratory (Grant No. LG-QS-202202-07).

Data availability statement The datasets generated during and/or analysed during the current study are available in the Imagenet (Deng et al., 2009) (<https://www.image-net.org/>), COCO (Lin et al., 2014) (https://cocodataset.org), ADE20K (Zhou et al., 2019) (<https://groups.csail.mit.edu/vision/datasets/ADE20K/>), Cityscapes (Cordts et al., 2016) (https://www.cityscapes-dataset.com), Long Range Arena (Tay et al., 2020) (<https://github.com/google-research/long-range-arena>) repositories.

A Nyström method

Nyström method Williams and Seeger (2000) aims to calculate a low-rank approximation for a Gram matrix. For Transformers, the self-attention matrix can be viewed as a Gram matrix S with a Gaussian kernel k applied to the query Q , with each element S_{ij} expressed as:

$$S_{ij} = k(Q_{i,:}, Q_{j,:}) = \exp\left(-\frac{\|Q_{i,:} - Q_{j,:}\|_2^2}{2\sqrt{d}}\right), \quad (18)$$

$k(x, y)$ means operating Gaussian kernel k to (x, y) , which can be written in the feature space as:

$$k(x, y) = \sum_{i=1}^n \lambda_i \phi_i(x) \phi_i(y), \quad (19)$$

n is the dimension of a feature space, λ_i denotes the eigenvalue and ϕ_i denotes the eigenfunction of kernel k . According to the eigenfunction’s definition, we can get:

$$\int k(y, x) \phi_i(x) p(x) dx = \lambda_i \phi_i(y), \quad (20)$$

where $p(x)$ is the probability distribution of x . And $\{\phi_i(x)\}$ are p -orthogonal:

$$\int \phi_i(x) \phi_j(x) p(x) dx = \delta_{ij}. \quad (21)$$

δ_{ij} is 0 when $i \neq j$, 1 when $i = j$. To get an approximation of the eigenfunctions, we sample $\{x_1, x_2, \dots, x_q\}$ from $p(x)$, then:

$$\frac{1}{q} \sum_{t=1}^q k(y, x_t) \phi_i(x_t) \approx \lambda_i \phi_i(y), \quad (22)$$

$$\frac{1}{q} \sum_{t=1}^q \phi_i(x_t) \phi_j(x_t) \approx \delta_{ij}. \quad (23)$$

This inspires us to approximate the Gram matrix S . Let $S^{(m)}$ be a submatrix of S , consisting of $m \times m$ elements from S . Gram matrix is a symmetric positive semi-definite matrix, so it has a spectral decomposition:

$$S^{(m)} U^{(m)} = U^{(m)} \Lambda^{(m)}, \quad (24)$$

where $U^{(m)}$ is column orthogonal and $\Lambda^{(m)}$ is a diagonal matrix with the diagonal elements as the eigenvalues of $S^{(m)}$. Substituting the y to x_j and applying the approximation above to S , we can get:

$$\phi_i(x_j) \approx \sqrt{m} U_{j,i}^{(m)}, \quad \lambda_i \approx \frac{\lambda_i^{(m)}}{m}, \quad (25)$$

$$\phi_i(y) \approx \frac{\sqrt{m}}{\lambda_i^{(m)}} \sum_{t=1}^m k(y, x_t) \phi_i(x_t), \quad (26)$$

λ_i is eigenvalue of S and $\lambda_i^{(m)}$ is the eigenvalue of $S^{(m)}$. Denote \tilde{S} as the rank- m approximation of S and $\tilde{U}, \tilde{\Lambda}$ as the

approximation for spectral decomposition of S . Now we can get an approximation of S with rank m :

$$\tilde{S} = \tilde{U} \tilde{\Lambda} \tilde{U}^T = \sum_{t=1}^m \tilde{\lambda}_t^{(n)} \tilde{u}_t^{(n)} (\tilde{u}_t^{(n)})^T. \quad (27)$$

Similarly, we have:

$$\phi_i(x_j) \approx \sqrt{n} U_{j,i}(n), \quad \lambda_i \approx \frac{\tilde{\lambda}_i^{(n)}}{n}. \quad (28)$$

Thus

$$\tilde{\lambda}_i^{(n)} \approx \frac{n \lambda_i^{(m)}}{m}, \quad (29)$$

$$\tilde{u}_t^{(n)} \approx \sqrt{\frac{m}{n}} \frac{1}{\lambda_t^{(m)}} S_{n,m} u_t^{(m)}. \quad (30)$$

Then we get an approximation of S : $\tilde{S} \approx S_{n,m} S_{m,m}^\dagger S_{m,n}$. S has a block representation below:

$$S = \begin{bmatrix} S_{m,m} & S_{m,n-m} \\ S_{n-m,m} & S_{n-m,n-m} \end{bmatrix}. \quad (31)$$

B Newton method

Proof of Proposition 1 When α is sufficiently small, $A_{k+1} = 2A_k - A_k A A_k$, A_k converges to A^\dagger .

Proof A is a symmetric positive semi-definite matrix and $A_{ij} \leq 1, \forall 1 \leq i, j \leq n, A_{ii} = 1, 1 \leq i \leq n$ in our case. A_0 is chosen to be αA , so the A_k can be written as $A_k = C_k A$ for some matrix C_k, D_k , leading to the fact that

$$A^\dagger A A_k = A_k, \quad A_k A A^\dagger = A_k. \quad (32)$$

This is because $A_{k+1} = A_k(2I_n - A A_k) = (2I_n - A_k A) A_k$ and $A_0 = \alpha A$. We make a difference between A^\dagger and A_{k+1} :

$$\begin{aligned} A^\dagger - A_{k+1} &= A^\dagger - 2A_k + A_k A A_k \\ &= A^\dagger - A_k A A^\dagger - A^\dagger A A_k + A_k A A_k \\ &= (A^\dagger - A_k) A (A^\dagger - A_k). \end{aligned} \quad (33)$$

We norm both sides of the equation above:

$$\begin{aligned} \|A^\dagger - A_{k+1}\| &= \|(A^\dagger - A_k) A (A^\dagger - A_k)\| \\ &\leq \|A^\dagger - A_k\| \|A (A^\dagger - A_k)\|. \end{aligned} \quad (34)$$

And we left multiply A on the both sides of (Eq 33), then norm the equation:

$$\begin{aligned} \|A A^\dagger - A A_{k+1}\| &= \|A (A^\dagger - A_k) A (A^\dagger - A_k)\| \\ &\leq \|A A^\dagger - A A_k\|^2. \end{aligned} \quad (35)$$

We choose α sufficiently small so that the initial value satisfy $\|A A^\dagger - A A_0\| < 1$. We set $\alpha = \frac{2}{\|A\|_1^2}$ to ensure it is small enough Ben-Israel and Cohen (1966). Then the $\|A A^\dagger - A A_k\| \rightarrow 0$, when $k \rightarrow \infty$. The inequality (34) implies that $A_k \rightarrow A^\dagger, k \rightarrow \infty$.

Proof of Equation 12

$$\nabla_x \mathcal{L} = -Y^\top (\nabla_Y \mathcal{L}) Y^\top,$$

Proof Since $XY = I$, we take derivatives on the both sides

$$\begin{aligned} Y dX + X dY &= 0 \\ dY &= -Y dX Y \end{aligned} \quad (36)$$

For the loss function \mathcal{L} , we have

$$d\mathcal{L} = \langle \nabla_X \mathcal{L}, dX \rangle = \langle \nabla_Y \mathcal{L}, dY \rangle$$

Recall that the inner product $\langle A, B \rangle = \text{Tr}(A^\top B)$ and $\text{Tr}(ABC) = \text{Tr}(CAB) = \text{Tr}(BCA)$, we have

$$\begin{aligned} \langle \nabla_X \mathcal{L}, dX \rangle &= \langle \nabla_Y \mathcal{L}, dY \rangle \\ &= \langle \nabla_Y \mathcal{L}, -Y dX Y \rangle \\ &= -\text{Tr}(\nabla_Y \mathcal{L}^\top Y dX Y) \\ &= \langle -Y^\top \nabla_Y \mathcal{L} Y^\top, dX \rangle \end{aligned}$$

Therefore, Eq (12) is proved.

C Attention normalization

Proof of Porpostion 5 Assume the bottleneck matrix of softmax-free attention, $A \in \mathbb{R}^{m \times m}$ is k -connected. If $\lambda_1 \geq \lambda_2 \geq \dots \geq \lambda_m \geq 0$ are eigenvalues of A^\dagger , then $\lambda_1 = \mathcal{O}(m^2)$ and $\|A^\dagger\|_2 = \mathcal{O}(m^2)$.

To prove Proposition 5, we first introduce the following lemmas.

Lemma 1 If F is a non-singular and symmetric matrix, then $\|F\|_2 \leq \|F\|_1$.

Proof According to the definition of 2-Norm, we have $F^T F z = \mu^2 z$ with $\mu = \|F\|_2$. Therefore, $\mu^2 \|z\|_1 = \|F^T F z\|_2 \leq \|F^T\|_1 \|F\|_1 \|z\|_1 = \|F\|_\infty \|F\|_1 \|z\|_1$. Since A is non-singular and symmetric,

$$\|F\|_2 \leq \sqrt{\|F\|_\infty \|F\|_1} = \|F\|_1 \quad (37)$$

Lemma 2 If F is a real matrix and $\|F\|_p < 1$, then

$$(I - F)^{-1} = \sum_{k=0}^{\infty} F^k \quad (38)$$

with

$$\|(I - F)^{-1}\|_p \leq \frac{1}{1 - \|F\|_p} \quad (39)$$

Proof

$$\left(\sum_{k=0}^N F^k \right) (I - F) = I - F^{N+1}$$

Since $\|F\|_p < 1, \lim_{k \rightarrow \infty} F^k = 0$. Thus,

$$\left(\lim_{N \rightarrow \infty} \sum_{k=0}^N F^k \right) (I - F) = I$$

Multiply the equation by $(I - F)^{-1}$ we obtain Eq (38). From that, we can easily get

$$\|(I - F)^{-1}\|_p \leq \sum_{k=0}^{\infty} \|F\|_p^k = \frac{1}{1 - \|F\|_p}$$

Now we begin to prove Proposition 5.

Proof Since the bottleneck matrix softmax-free attention $\|A\|_1$ is not less than 1, we normalize the matrix as $A_n = D^{-1}A$, where $D = \text{diag}(A\mathbb{1}_m)$. From Lemma 2, it follows that

$$\|A_n^{-1}\|_1 \leq \frac{1}{1 - \|I - A_n\|_1}$$

Since we assume the bottleneck matrix is k -connected, and $k \ll m$,

$$\|I - A_n\|_1 \leq \frac{(m - k)}{m}$$

Then,

$$\|A_n^{-1}\|_1 \leq \frac{1}{1 - \frac{(m-k)}{m}} = \frac{m}{k} = \mathcal{O}(m)$$

Note that we $D = \mathcal{O}(m)$ by assumption that the bottleneck matrix is k -connected, it follows that

$$\|A^{-1}\|_1 = \|A_n^{-1}D\|_1 \leq \|A_n^{-1}\|_1 \|D\|_1 = \mathcal{O}(m^2)$$

D Non-linearized Gaussian kernel attention

Instead of directly calculating the Gaussian kernel weights, in our formulation they are approximated. More specifically, the relation between any two tokens is reconstructed via sampled bottleneck tokens. As the number m (*e.g.*, 49) of bottleneck tokens is much smaller than the entire token sequence length, our attention matrix is of low-rank. This brings about two favorable consequences: **(I)** The model now focuses the attentive learning on latent salient information captured by the m bottleneck tokens. **(II)** The model becomes more robust against the underlying token noise due to the auto-encoder style reconstruction Geng et al. (2021). This explains why a model with an approximated gram matrix performs better than one with a directly computed matrix. Further, we find that exact Gaussian kernel attention leads to training difficulties. As Proposition 4 reveals, this is due to lacking normalization that leads to explosion of the spectral norm especially in long token sequence cases. Big spectral norm could jeopardize the training and tend to collapse the model.

E Attention visualization

Figure 7 shows more visualization of the attention masks by various Transformers Choromanski et al. (2021), Vaswani et al. (2017), Xiong et al. (2021) and our SOFT. For each model, we show the output from the first two attention heads (up and down row). It is noteworthy that SOFT exhibits better semantic diversity of the multi-head mechanism than other methods. Moreover, when we sample the patch at the boundary of multiple objects, SOFT is able to more precisely capture all these objects.

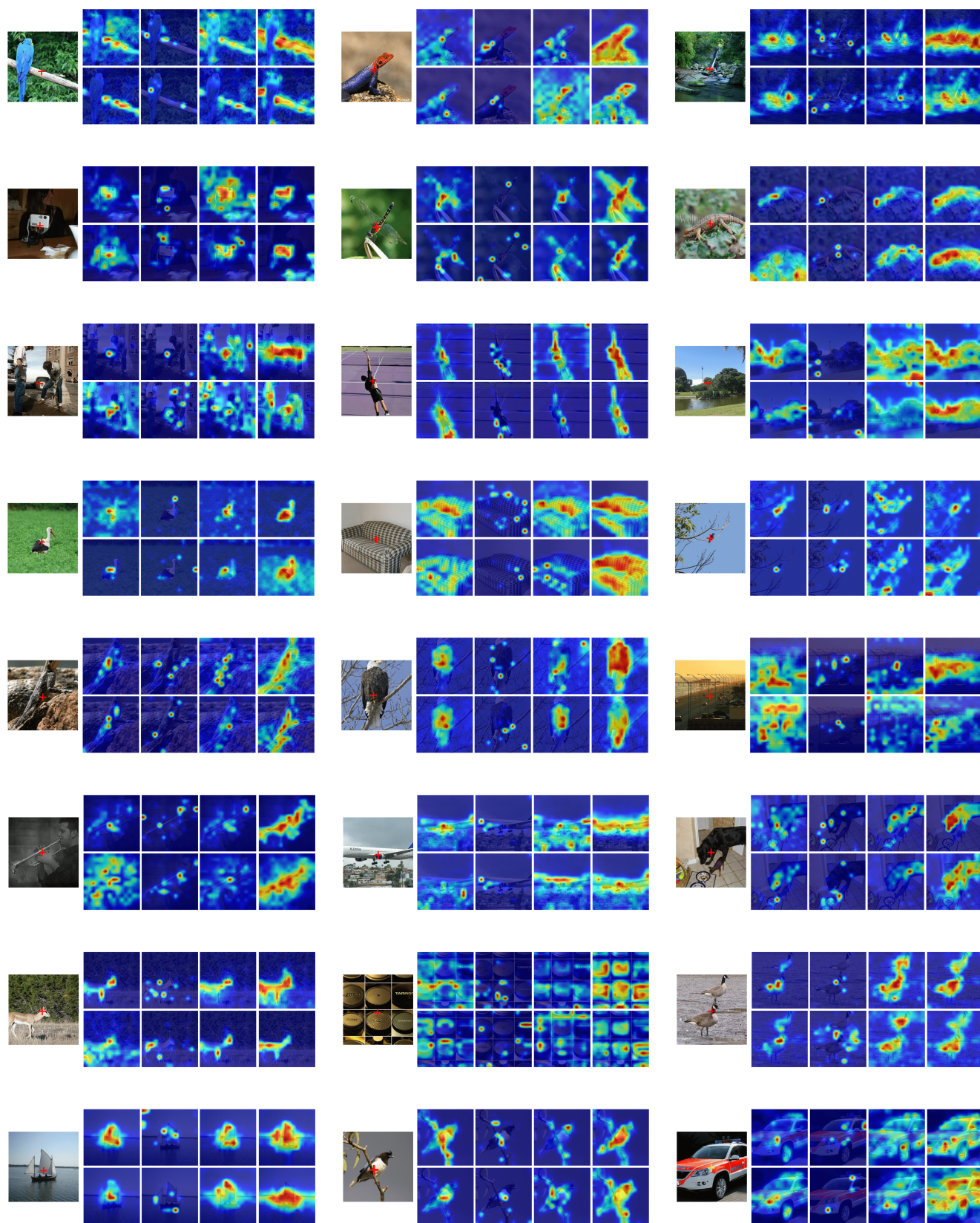


Fig. 7 Comparison of attention heatmaps for a selected query patch (indicated by a cross "+") against all patches in an image. Heatmaps are derived from the first head's corresponding row in the attention maps, as calculated by Equation 17. These heatmaps are normalized to a 0-1 scale, with warmer colors indicating higher relevance. The model variants compared are: (a) Transformer (Vaswani et al., 2017), (b) Performer (Choromanski et al., 2021), (c) Nystromformer (Xiong et al., 2021), and (d) Our SOFT approach.

References

- Ba JL, Kiros JR, Hinton GE (2016) Layer normalization. arXiv preprint arXiv:160706450
- Bello I (2021) Lambdanetworks: Modeling long-range interactions without attention. In: International Conference on Learning Representations
- Ben-Israel A, Cohen D (1966) On iterative computation of generalized inverses and associated projections. *SIAM Journal on Numerical Analysis* 3(3):410–419
- Brown T, Mann B, Ryder N, Subbiah M, Kaplan JD, Dhariwal P, Neelakantan A, Shyam P, Sastry G, Askell A, et al. (2020) Language models are few-shot learners. *Advances in Neural Information Processing Systems* 33:1877–1901
- Chen K, Wang J, Pang J, Cao Y, Xiong Y, Li X, Sun S, Feng W, Liu Z, Xu J, et al. (2019) Mmdetection: Open mmlab detection toolbox and benchmark. arXiv preprint arXiv:190607155
- Chen LC, Zhu Y, Papandreou G, Schroff F, Adam H (2018) Encoder-decoder with atrous separable convolution for semantic image segmentation. In: European Conference on Computer Vision, pp 801–818
- Cheng J, Grossman M, McKercher T (2014) Professional CUDA c programming
- Choromanski K, Likhoshesterov V, Dohan D, Song X, Gane A, Sarlos T, Hawkins P, Davis J, Mohiuddin A, Kaiser L, et al. (2021) Rethinking attention with performers. In: International Conference on Learning Representations
- Chu X, Tian Z, Wang Y, Zhang B, Ren H, Wei X, Xia H, Shen C (2021) Twins: Revisiting the design of spatial attention in vision transformers. *Advances in Neural Information Processing Systems* 34:9355–9366
- Cordts M, Omran M, Ramos S, Rehfeld T, Enzweiler M, Benenson R, Franke U, Roth S, Schiele B (2016) The cityscapes dataset for semantic urban scene understanding. In: IEEE Conference on Computer Vision and Pattern Recognition, pp 3213–3223
- Dai Z, Liu H, Le QV, Tan M (2021) Coatnet: Marrying convolution and attention for all data sizes. In: *Advances in Neural Information Processing Systems*, vol 34, pp 3965–3977
- Deng J, Dong W, Socher R, Li LJ, Li K, Fei-Fei L (2009) Imagenet: A large-scale hierarchical image database. In: IEEE Conference on Computer Vision and Pattern Recognition, pp 248–255
- Devlin J, Chang MW, Lee K, Toutanova K (2019) Bert: Pre-training of deep bidirectional transformers for language understanding. In: Conference of the North American Chapter of the Association for Computational Linguistics: Human Language Technologies, NAACL-HLT, pp 4171–4186
- Dosovitskiy A, Beyer L, Kolesnikov A, Weissenborn D, Zhai X, Unterthiner T, Dehghani M, Minderer M, Heigold G, Gelly S, et al. (2021) An image is worth 16x16 words: Transformers for image recognition at scale. In: International Conference on Learning Representations
- d’Ascoli S, Touvron H, Leavitt ML, Morcos AS, Biroli G, Sagun L (2021) Convit: Improving vision transformers with soft convolutional inductive biases. In: International Conference on Machine Learning, PMLR, pp 2286–2296
- Fasshauer GE (2011) Positive definite kernels: past, present and future. *Dolomites Research Notes on Approximation* 4:21–63
- Geng Z, Guo MH, Chen H, Li X, Wei K, Lin Z (2021) Is attention better than matrix decomposition? In: International Conference on Learning Representations
- Guo MH, Liu ZN, Mu TJ, Hu SM (2022) Beyond self-attention: External attention using two linear layers for visual tasks. *IEEE Transactions on Pattern Analysis and Machine Intelligence* 45(5):5436–5447
- He K, Zhang X, Ren S, Sun J (2016) Deep residual learning for image recognition. In: IEEE Conference on Computer Vision and Pattern Recognition, pp 770–778
- He K, Gkioxari G, Dollár P, Girshick R (2017) Mask r-cnn. In: IEEE International Conference on Computer Vision, pp 2961–2969
- Huang Z, Wang X, Huang L, Huang C, Wei Y, Liu W (2019) Ccnet: Criss-cross attention for semantic segmentation. In: IEEE International Conference on Computer Vision, pp 603–612
- Ioffe S, Szegedy C (2015) Batch normalization: Accelerating deep network training by reducing internal covariate shift. In: International Conference on Machine Learning, pmlr, pp 448–456
- Jaegle A, Gimeno F, Brock A, Vinyals O, Zisserman A, Carreira J (2021) Perceiver: General perception with iterative attention. In: International Conference on Machine Learning, PMLR, pp 4651–4664
- Kasai J, Peng H, Zhang Y, Yogatama D, Ilharco G, Pappas N, Mao Y, Chen W, Smith NA (2021) Fine-tuning pretrained transformers into rnns. In: Conference on Empirical Methods in Natural Language Processing, pp 10630–10643
- Katharopoulos A, Vyas A, Pappas N, Fleuret F (2020) Transformers are rnns: Fast autoregressive transformers with linear attention. In: International Conference on Machine Learning, PMLR, pp 5156–5165
- Kitaev N, Kaiser L, Levskaya A (2020) Reformer: The efficient transformer. In: International Conference on

- Learning Representations
- Krizhevsky A (2009) Learning multiple layers of features from tiny images. URL <https://api.semanticscholar.org/CorpusID:18268744>
- Lin TY, Maire M, Belongie S, Hays J, Perona P, Ramanan D, Dollár P, Zitnick CL (2014) Microsoft coco: Common objects in context. In: European Conference on Computer Vision, Springer, pp 740–755
- Lin TY, Goyal P, Girshick R, He K, Dollár P (2017) Focal loss for dense object detection. In: IEEE International Conference on Computer Vision, pp 2980–2988
- Liu Z, Lin Y, Cao Y, Hu H, Wei Y, Zhang Z, Lin S, Guo B (2021) Swin transformer: Hierarchical vision transformer using shifted windows. In: Proceedings of the IEEE/CVF international conference on computer vision, pp 10012–10022
- Liu Z, Hu H, Lin Y, Yao Z, Xie Z, Wei Y, Ning J, Cao Y, Zhang Z, Dong L, et al. (2022a) Swin transformer v2: Scaling up capacity and resolution. In: IEEE Conference on Computer Vision and Pattern Recognition, pp 12009–12019
- Liu Z, Mao H, Wu CY, Feichtenhofer C, Darrell T, Xie S (2022b) A convnet for the 2020s. In: IEEE Conference on Computer Vision and Pattern Recognition, pp 11976–11986
- Long J, Shelhamer E, Darrell T (2015) Fully convolutional networks for semantic segmentation. In: IEEE Conference on Computer Vision and Pattern Recognition, pp 3431–3440
- Lu J, Yao J, Zhang J, Zhu X, Xu H, Gao W, Xu C, Xiang T, Zhang L (2021) Soft: softmax-free transformer with linear complexity. *Advances in Neural Information Processing Systems* 34:21297–21309
- Maas A, Daly RE, Pham PT, Huang D, Ng AY, Potts C (2011) Learning word vectors for sentiment analysis. In: Proceedings of the 49th annual meeting of the association for computational linguistics: Human language technologies, pp 142–150
- Mindspore (2020) <https://www.mindspore.cn/>
- Nangia N, Bowman SR (2018) Listops: A diagnostic dataset for latent tree learning. In: Conference of the North American Chapter of the Association for Computational Linguistics, Student Research Workshop, pp 92–99
- Peng H, Pappas N, Yogatama D, Schwartz R, Smith NA, Kong L (2021) Random feature attention. In: International Conference on Learning Representations
- Radev DR, Muthukrishnan P, Qazvinian V, Abu-Jbara A (2013) The acl anthology network corpus. *Language Resources and Evaluation* 47:919–944
- Radosavovic I, Kosaraju RP, Girshick R, He K, Dollár P (2020) Designing network design spaces. In: IEEE Conference on Computer Vision and Pattern Recognition, pp 10428–10436
- Sun S, Yue X, Bai S, Torr P (2021) Visual parser: Representing part-whole hierarchies with transformers. arXiv preprint arXiv:210705790
- Szegedy C, Vanhoucke V, Ioffe S, Shlens J, Wojna Z (2016) Rethinking the inception architecture for computer vision. In: IEEE Conference on Computer Vision and Pattern Recognition, pp 2818–2826
- Tay Y, Dehghani M, Abnar S, Shen Y, Bahri D, Pham P, Rao J, Yang L, Ruder S, Metzler D (2020) Long range arena: A benchmark for efficient transformers. In: International Conference on Learning Representations
- Tay Y, Dehghani M, Bahri D, Metzler D (2023) Efficient transformers: A survey. *ACM Computing Surveys* 55(6):109:1–109:28
- Touvron H, Cord M, Douze M, Massa F, Sablayrolles A, Jégou H (2021a) Training data-efficient image transformers & distillation through attention. In: International Conference on Machine Learning, PMLR, pp 10347–10357
- Touvron H, Cord M, Sablayrolles A, Synnaeve G, Jégou H (2021b) Going deeper with image transformers. In: IEEE Conference on Computer Vision and Pattern Recognition, pp 32–42
- Touvron H, Cord M, Jégou H (2022) Deit iii: Revenge of the vit. In: European Conference on Computer Vision, pp 516–533
- Tsai YHH, Bai S, Yamada M, Morency LP, Salakhutdinov R (2019) Transformer dissection: A unified understanding of transformer’s attention via the lens of kernel. In: Conference on Empirical Methods in Natural Language Processing and International Joint Conference on Natural Language Processing (EMNLP-IJCNLP), pp 4344–4353
- Vaswani A, Shazeer N, Parmar N, Uszkoreit J, Jones L, Gomez AN, Kaiser Ł, Polosukhin I (2017) Attention is all you need. *Advances in Neural Information Processing Systems* 30
- Von Luxburg U (2007) A tutorial on spectral clustering. *Statistics and computing* 17:395–416
- Wang S, Li BZ, Khabsa M, Fang H, Ma H (2020) Linformer: Self-attention with linear complexity. arXiv preprint arXiv:200604768
- Wang W, Xie E, Li X, Fan DP, Song K, Liang D, Lu T, Luo P, Shao L (2021) Pyramid vision transformer: A versatile backbone for dense prediction without convolutions. In: IEEE International Conference on Computer Vision, pp 568–578
- Wang W, Xie E, Li X, Fan DP, Song K, Liang D, Lu T, Luo P, Shao L (2022) Pvt v2: Improved baselines with pyramid vision transformer. *Computational Vi-*

- sual Media 8(3):415–424
- Wang X, Girshick R, Gupta A, He K (2018) Non-local neural networks. In: IEEE Conference on Computer Vision and Pattern Recognition, pp 7794–7803
- Wightman R (2019) Pytorch image models. <https://github.com/rwightman/pytorch-image-models>
- Williams C, Seeger M (2000) Using the nyström method to speed up kernel machines. *Advances in Neural Information Processing Systems* 13
- Xiao T, Liu Y, Zhou B, Jiang Y, Sun J (2018) Unified perceptual parsing for scene understanding. In: European Conference on Computer Vision, pp 418–434
- Xie S, Girshick R, Dollár P, Tu Z, He K (2017) Aggregated residual transformations for deep neural networks. In: IEEE Conference on Computer Vision and Pattern Recognition, pp 1492–1500
- Xiong Y, Zeng Z, Chakraborty R, Tan M, Fung G, Li Y, Singh V (2021) Nyströmformer: A nyström-based algorithm for approximating self-attention. In: AAAI Conference on Artificial Intelligence, vol 35, pp 14138–14148
- Xu W, Xu Y, Chang T, Tu Z (2021) Co-scale convolutional image transformers. In: Proceedings of the IEEE/CVF International Conference on Computer Vision, pp 9981–9990
- Yoshida Y, Miyato T (2017) Spectral norm regularization for improving the generalizability of deep learning. arXiv preprint arXiv:170510941
- Yuan L, Chen Y, Wang T, Yu W, Shi Y, Jiang ZH, Tay FE, Feng J, Yan S (2021) Tokens-to-token vit: Training vision transformers from scratch on imagenet. In: IEEE International Conference on Computer Vision, pp 558–567
- Yuan Y, Chen X, Wang J (2020) Object-contextual representations for semantic segmentation. In: European Conference on Computer Vision, pp 173–190
- Yun S, Han D, Oh SJ, Chun S, Choe J, Yoo Y (2019) Cutmix: Regularization strategy to train strong classifiers with localizable features. In: IEEE International Conference on Computer Vision, pp 6023–6032
- Zhang H, Cissé M, Dauphin YN, Lopez-Paz D (2018) mixup: Beyond empirical risk minimization. In: International Conference on Learning Representations
- Zhang L, Xu D, Arnab A, Torr PH (2020) Dynamic graph message passing networks. In: IEEE Conference on Computer Vision and Pattern Recognition, pp 3726–3735
- Zhang P, Dai X, Yang J, Xiao B, Yuan L, Zhang L, Gao J (2021) Multi-scale vision longformer: A new vision transformer for high-resolution image encoding. In: IEEE International Conference on Computer Vision, pp 2998–3008
- Zhao H, Shi J, Qi X, Wang X, Jia J (2017) Pyramid scene parsing network. In: IEEE Conference on Computer Vision and Pattern Recognition, pp 2881–2890
- Zhao H, Jia J, Koltun V (2020) Exploring self-attention for image recognition. In: IEEE Conference on Computer Vision and Pattern Recognition, pp 10076–10085
- Zheng S, Lu J, Zhao H, Zhu X, Luo Z, Wang Y, Fu Y, Feng J, Xiang T, Torr PH, et al. (2021) Rethinking semantic segmentation from a sequence-to-sequence perspective with transformers. In: IEEE Conference on Computer Vision and Pattern Recognition, pp 6881–6890
- Zhou B, Zhao H, Puig X, Xiao T, Fidler S, Barriuso A, Torralla A (2019) Semantic understanding of scenes through the ade20k dataset. *International Journal of Computer Vision* 127:302–321
- Zhu X, Su W, Lu L, Li B, Wang X, Dai J (2021) Deformable detr: Deformable transformers for end-to-end object detection. In: International Conference on Learning Representations